

MK-SGN: A Spiking Graph Convolutional Network with Multimodal Fusion and Knowledge Distillation for Skeleton-based Action Recognition

Naichuan Zheng^{1a}, Hailun Xia^{21a}, Zeyu Liang^{3a}, Yuchen Du^{4a}

^aBeijing Laboratory of Advanced Information Networks, Beijing Key Laboratory of Network System Architecture and Convergence, School of Information and Communication Engineering, Beijing University of Posts and Telecommunications, , Beijing, 100876, , China

Abstract

In recent years, multimodal Graph Convolutional Networks (GCNs) have achieved remarkable performance in skeleton-based action recognition. The reliance on high-energy-consuming continuous floating-point operations inherent in GCN-based methods poses significant challenges for deployment in energy-constrained, battery-powered edge devices. To address these limitations, MK-SGN, a Spiking Graph Convolutional Network with Multimodal Fusion and Knowledge Distillation, is proposed to leverage the energy efficiency of Spiking Neural Networks (SNNs) for skeleton-based action recognition for the first time. By integrating the energy-saving properties of SNNs with the graph representation capabilities of GCNs, MK-SGN achieves significant reductions in energy consumption while maintaining competitive recognition accuracy. Firstly, we formulate a Spiking Multimodal Fusion (SMF) module to effectively fuse multimodal skeleton data represented as spike-form features. Secondly, we propose the Self-Attention Spiking Graph Convolution (SA-SGC) module and the Spiking Temporal Convolution (STC) module, to capture spatial relationships and temporal dynamics of spike-form features. Finally, we propose an integrated knowledge distillation strategy to transfer information from the multimodal GCN to the SGN, incorporating both intermediate-layer distillation and soft-label distillation to enhance the performance of the SGN. MK-SGN exhibits substantial advantages, surpassing state-of-the-art GCN frameworks in energy efficiency and outperforming state-of-the-art SNN frameworks in recognition accuracy. The proposed method achieves a remarkable reduction in energy consumption, exceeding 98% compared to conventional GCN-based approaches. This research establishes a robust baseline for developing high-performance, energy-efficient SNN-based models for skeleton-based action recognition

Keywords:

Spiking Graph Convolution Network, Multimodal, Knowledge Distillation, Skeleton-based Action Recognition

1. Introduction

Human action recognition is a critical task with wide-ranging applications in human-computer interaction, identity verification, and emergency detection [1]. Initial approaches predominantly relied on RGB-based methods that analyzed visual information extracted from video frames[2]. While effective in certain contexts, such methods encountered significant challenges in complex environments characterized by cluttered backgrounds, inadequate lighting, and occlusions, limiting their robustness and generalization capabilities. To address limitations in earlier approaches, research has shifted towards skeleton-based action recognition, which utilizes 3D skeleton data obtained from depth sensors [3]. By isolating human action dynamics from environmental disturbances, skeleton-based recognition enhances robustness and reliability in action recognition tasks. Early methods employed Convolutional Neural Networks (CNNs) [4, 5, 6], Recurrent Neural Networks (RNNs) [8, 7], and Long Short-Term Memory networks

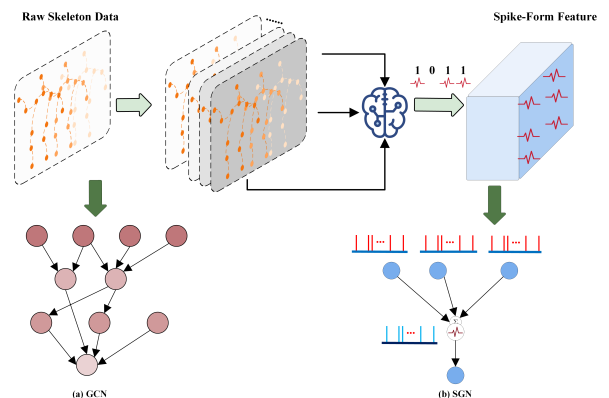


Figure 1: Comparison of (a) GCN and (b) SGN for skeleton-based Action Recognition. The former performs feature extraction and information propagation on nodes of the graph structure through graph convolutional layers, while the latter employs spike encoding to convert features into discrete spike-form, conducting feature extraction and information propagation in the time dimension of the spike-form feature.

Email addresses: 2022110134zhengnaichuan@bupt.edu.cn (Naichuan Zheng¹), xiahailun@bupt.edu.cn (Hailun Xia²), lzy_sfading@bupt.edu.cn (Zeyu Liang³), duyuchen@bupt.edu.cn (Yuchen Du⁴)

Networks (GCNs), which represent a significant advancement in the field [10].

GCNs effectively model the spatial and temporal relationships within skeleton data, with the introduction of ST-GCN representing a key milestone [11]. The architecture employs spatial-temporal graph convolution to process skeletal data and laid the foundation for more advanced frameworks. 2S-AGCN improved performance by integrating a two-stream structure (Joint and Bone Streams) alongside adaptive graph convolution, enabling dynamic learning of skeletal topologies and refinement of temporal features [12]. Subsequent advancements aimed to balance efficiency and accuracy. Shift-GCN utilized a Channel-wise Shift Operation to simulate spatio-temporal information flow with minimal computational overhead [13], whereas CTR-GCN introduced channel-level topology optimization and attention mechanisms to enhance feature representation [14]. Building on foundational models, InfoGCN leverages information bottleneck theory for representation learning and extends the skeleton modality to six streams using the k-hop approach [15]. The development culminated in HULK, a multimodal large-scale model designed to unify diverse modalities within a robust framework. By harnessing its extensive capacity, HULK achieves state-of-the-art (SOTA) performance in precision and multimodal integration [16].

However, such performance in traditional methods often relies on deep network architectures typical of artificial neural networks (ANNs), which are heavily dependent on computationally expensive floating-point operations. Such reliance results in considerable computational energy demands. For example, lightweight models like Shift-GCN and CTR-GCN consume 46 mJ and 36.25 mJ per action sample, respectively, while 2S-AGCN requires up to 164.68 mJ per sample (single-sample energy consumption calculated based on Equation 37). Additionally, the pursuit of improved accuracy necessitates the integration of multimodal data, which requires separate training and testing for each modality, followed by ensemble fusion. These approaches significantly increase both computational complexity and energy consumption, posing substantial challenges for deployment on battery-powered edge devices and other energy-constrained environments

To address the high energy consumption and deployment challenges associated with ANN-based methods, Spiking Neural Networks (SNNs) provide a promising alternative, renowned for their energy efficiency [17]. Inspired by biomimetics, SNNs utilize event-driven mechanisms that enable exceptionally low energy consumption, making them particularly well-suited for resource-constrained environments. The energy-efficient design positions SNNs as a viable solution to the limitations of traditional ANN frameworks in practical applications [18, 19, 20]. SNNs have evolved significantly alongside advancements in ANNs, incorporating advanced architectures such as Spiking Graph Neural Networks [21, 22, 23], Spiking Recurrent Neural Networks [24, 25, 26], and Spiking Transformers [27, 28, 29]. Research efforts have primarily focused on tasks such as RGB image classification [51] and event-driven recognition [30, 31, 32], achieving notable success in reducing energy consumption while maintain-

ing high accuracy.

Building on advancements in SNNs and GCNs, we propose a novel Spiking Graph Network (SGN) framework that, for the first time, integrates the energy efficiency of SNNs with the graph representation capabilities of GCNs for skeleton-based action recognition. Our work revolutionizes skeleton-based action recognition by establishing the first framework based on SNNs, unveiling their transformative potential in addressing diverse real-world challenges, particularly in environments with strict energy constraints.

The exploration of SGNs for skeleton action recognition is guided by several scientific challenges that prompt deep reflection:

1. **Transformation of Skeleton Data into Spike-based Representations:** What methodologies can effectively transform skeleton data, characterized by complex graphical structures, into spike-based representations compatible with the computational principles of SNNs?
2. **Multimodal Feature Fusion within SNNs:** What advanced techniques can facilitate the fusion of multimodal features in SNNs, ensuring consistency, coherence, and resilience in feature representation?
3. **Compatibility with Vanilla GCNs:** How can spike-based representations be effectively integrated with vanilla GCNs to ensure seamless functionality and robust performance in action recognition tasks?
4. **Optimization of Energy Efficiency and Accuracy:** What strategies can be employed to optimize the trade-off between energy consumption and recognition accuracy, achieving a balance that meets the requirements of energy-constrained environments?

The identified challenges emphasize crucial areas for innovation, driving progress at the intersection of SNNs and GCNs for achieving both energy-efficient and highly accurate action recognition. To address these issues, we first propose a Skeleton Spiking Coding (SSC) module to convert skeleton data into event spikes and a Spike-based Multimodal Fusion (SMF) module based on mutual information to compute the correlation between multimodal data for early fusion. The SMF module fully leverages the complementary information from multimodal skeleton data while avoiding the heavy training and testing burden associated with ensemble methods. Building on these components, we further develop a novel SGN block, which integrates Self-Attention-Spiking Graph Convolutions (SA-SGC) and Spiking Temporal Convolutions (STC). The SA-SGC employs a spiking attention mechanism to enhance the representation of spiking features, thereby improving classification performance. Meanwhile, the STC extracts temporal features from spike-form data derived from skeleton sequences, capturing fine-grained temporal dependencies to complement the spatial information encoded by the SA-SGC. This integrated design bridges the gap between SGN and traditional GCN in feature extraction and information propagation. Additionally, a GCN-to-SGN knowledge distillation method is formulated, comprising inner-layer feature distillation and soft label distillation. High-precision GCN models guide the training of SGN

through these complementary strategies. A Feature Translation Module (FTM) is employed to convert inner-layer features from multimodal GCN into spike-form features, enabling effective inner-layer feature distillation. Soft label distillation transfers the output distribution knowledge from GCN to SGN, further enhancing model performance. The dual-distillation approach improves accuracy without increasing model complexity. Leveraging the maturity of GCN architectures and pre-trained weights, the process imposes no additional training burden. Ultimately, we propose Spiking Graph Convolutional Network with Multimodal Fusion and Knowledge Distillation (MK-SGN), the first framework to leverage SNNs for addressing skeleton-based action recognition. Extensive experiments validate the effectiveness of the proposed approach, demonstrating its ability to achieve energy-efficient and accurate performance while bridging the gap between SNNs and GCNs in this domain.

Overall, the main contributions of this paper can be summarized as follows:

(1) A novel MK-SGN framework is proposed, introducing skeleton-based action recognition into the domain of SNNs and establishing a foundation for future research in energy-efficient action recognition.

(2) An SMF module is formulated to fuse multimodal skeleton data in the form of spike-form features based on mutual information, effectively integrating complementary information while minimizing energy consumption and computational overhead. The novel SA-SGC and STC modules further enhance the representation of spatial relationships and temporal dynamics within the fused spike-form features.

(3) A knowledge distillation strategy is formulated to transfer knowledge from GCN to SGN, integrating both inner-layer feature distillation and soft label distillation for heterogeneous networks. To enable effective intermediate layer distillation, an FTM is designed to convert features from the intermediate layers of multimodal GCN into spike-form representations.

(4) Extensive experiments on three challenging datasets demonstrate the advantages of our work. The theoretical energy consumption of MK-SGN is **0.614 mJ per action sample**. Compared to SOTA GCN-based methods, it **reduces energy consumption by more than 98%**. Moreover, we surpass the accuracy of SOTA SNN-based methods.

2. Related Work

2.1. Skeleton-based Action Recognition

In recent years, deep learning has significantly advanced skeleton-based action recognition [3]. Early research on skeleton data primarily uses CNNs to extract spatial features, focusing on patterns such as joint positions and spatial relationships [4, 5, 6]. RNNs, including the more advanced variant LSTMs, model temporal dynamics, capturing sequential dependencies in movement patterns over time. Such methods address spatial and temporal dimensions separately, with LSTMs excelling at learning long-term dependencies in motion sequences [8, 7, 34, 35, 36]. However, CNN- and RNN-based

approaches fail to adequately exploit the graph-like structure of skeleton data, limiting their capacity to represent joint dependencies and hierarchical relationships fully. The introduction of ST-GCN marked a breakthrough by representing skeletons as graphs, enabling the explicit modeling of spatio-temporal relationships through graph convolutions [11]. Since then, numerous studies have aimed to improve GCN performance, focusing on both spatial and temporal modeling. In the spatial domain, methods have primarily focused on capturing intrinsic joint correlations through techniques such as learnable adjacency matrices [41, 42, 43], attention mechanisms [37, 38, 39, 40], and other adaptive strategies, to enhance spatial feature representations by dynamically modeling relationships between joints, thereby overcoming the limitations of static graph structures. In the temporal domain, methods have focused on improving the temporal receptive fields to effectively capture both long-term and short-term dependencies, employing multi-stage strategies to model complex action dynamics and achieve finer-grained temporal representations [14, 44]. The integration of multimodal skeleton data, including joint, bone, motion, and additional dynamic features, has significantly advanced the field. By leveraging complementary modalities, methods such as Shift-GCN, CTR-GCN, and Info-GCN enhance recognition performance [13, 14, 15]. The development culminated in Hulk [16], a multimodal large-scale model that unified diverse modalities into a comprehensive framework, achieving SOTA results. Despite advancements in skeleton-based action recognition, current methods rely on ANN-based architectures, which require significant floating-point operations and lead to high energy consumption. Although effective, scalability and energy efficiency remain challenges. SNNs present a potential solution but have yet to be explored in this context, leaving a notable gap in the research.

2.2. Spiking Neural Networks

Unlike ANNs, SNNs transmit information through discrete spike sequences, a mechanism inspired by biological principles. This spike-driven mode closely mimics brain function, offering significant potential for energy efficiency [17]. Early research in SNNs focused on various spiking neuron models designed to convert continuous inputs into spike sequences. Notable models include the Integrate-and-Fire (IF) neuron [45], which simplifies the process by accumulating input signals until a threshold is reached, and the Hodgkin-Huxley (HH) model [46], which provides a biophysically detailed representation of neuronal activity based on ion channel dynamics. The Leaky Integrate-and-Fire (LIF) neuron is widely regarded for its simplicity and efficiency [47]. The dynamics and update of the membrane potential are described as:

$$\tau_m \frac{dV}{dt} = -(V - V_{\text{rest}}) + R \cdot I(t), \quad (1)$$

$$V(t + \Delta t) = \begin{cases} V_{\text{reset}}, & \text{if } V(t) \geq V_{\text{thresh}} \\ V(t) + \left(\frac{-(V(t) - V_{\text{rest}}) + I(t)}{\tau_m} \right) \Delta t, & \text{otherwise} \end{cases}, \quad (2)$$

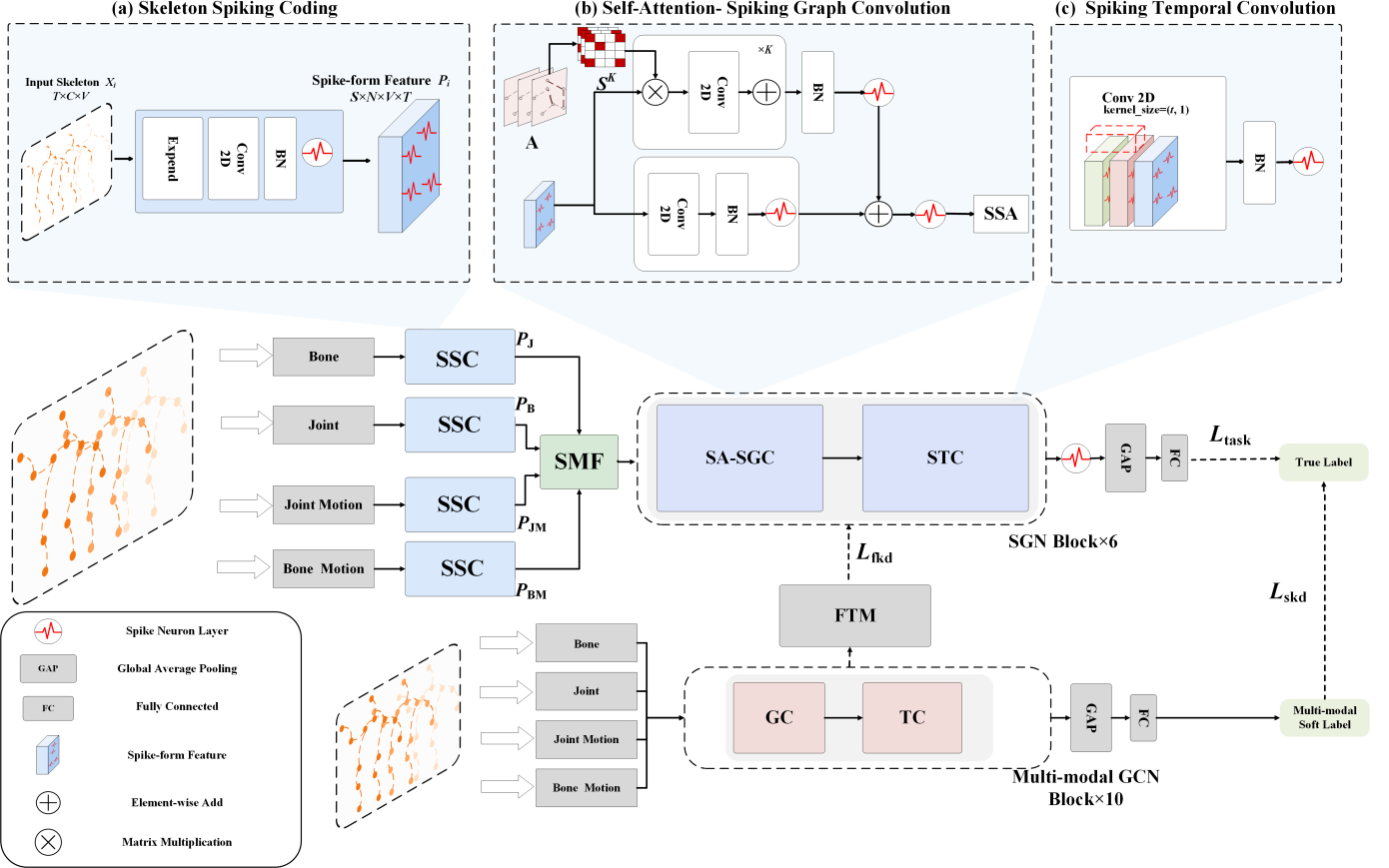


Figure 2: The overview of the proposed network architecture. The teacher network consists of a 10-layer GCN that processes four multimodal skeleton datasets independently, followed by Global Average Pooling (GAP) and Fully Connected (FC) layers to generate soft labels. The student network is a 6-layer SGN that incorporates the following key modules: (a) The Spiking Coding Module (SSC), which transforms raw skeleton data into spike-form representations, enabling compatibility with spiking neural computations. (b) The Spiking Self-Attention Spiking Graph Convolution (SA-SGC) module, formulated to model the spatio-temporal dependencies within spike-form features effectively by combining self-attention and spiking graph convolution. (c) The Spiking Temporal Convolution (STC) module, which captures temporal patterns and refines temporal dynamics within spike-form features. Additionally, the Spike-based Multimodal Fusion Module (SMF) optimizes cross-modal integration using mutual information, and the Feature Transformation Module (FTM) maps inter-layer GCN features into spike-form representations for effective alignment with the SNN domain. Knowledge distillation is achieved through the FTM and supervision from the soft labels produced by the teacher network.

where $V(t)$ represents the membrane potential at the current time point, where V_{rest} denotes the neuron’s resting potential. $I(t)$ indicates the input current. The membrane time constant is given by τ_m , and V_{thresh} is the threshold potential that triggers the firing of an action potential. After firing, the membrane potential is reset to V_{reset} . The model’s discrete update time step is Δt .

These advancements have led to the development of various spiking neural architectures, such as Spiking Graph Convolutional Networks [21, 22, 23], Spiking Transformers [27, 28, 29], Spiking Recurrent Neural Networks [24, 25, 26], and Spiking Convolutional Neural Networks [48, 49]. While existing research has primarily focused on traditional ANN tasks, significant progress has been made in spiking adaptations of Transformer models, particularly for RGB image processing. Studies in this area have demonstrated substantial energy savings without compromising accuracy [51]. Other research has focused on event-driven recognition, which is particularly well-suited for SNNs due to their ability to process sparse and asyn-

chronous data [50]. Although SNNs have made significant progress in other areas, their application to skeleton-based action recognition remains underexplored. The event-driven nature of SNNs provides a promising approach to significantly improving energy efficiency, albeit with a certain trade-off in accuracy. Leveraging this potential could provide a viable solution to the challenge of balancing energy efficiency and accuracy in action recognition tasks.

3. Proposed Method

This section begins with the comprehensive architectural design of the MK-SGN, followed by an introduction to its Spiking Coding mechanism, the Spiking Multimodal Fusion Module, SGN Block and the Knowledge Distillation Method from GCN to SGN are then described in detail.

3.1. Overall Architecture

Our network architecture, illustrated in Figure 2, comprises a 10-layer multimodal teacher GCN network and a 6-layer SNN

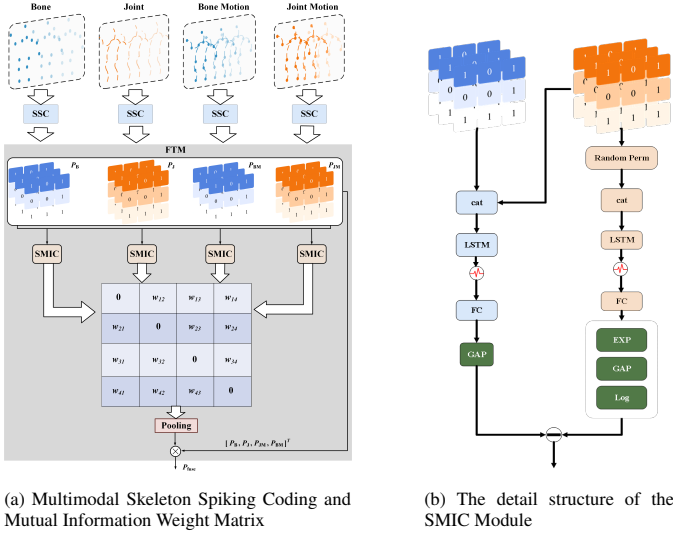


Figure 3: Multimodal Skeleton Spiking Coding and Mutual Information Weight Matrix Calculation Process

student network. The teacher GCN network processes the four multimodal skeleton datasets separately. The processed features from each modality are then passed through the Global Average Pooling (GAP) and Fully Connected (FC) layers to generate predictions. These predictions are finally fused to produce the soft labels.

The student SGN network processes each modality independently through the SSC module, transforming skeleton data into spike-form representations. Spike-form features are then fused via the SMF module, utilizing mutual information to optimize cross-modal integration. Each student network layer includes an SA-SGC module and a STC module, which are designed to capture and refine temporal and spatial features efficiently and effectively. Our approach implements knowledge distillation through inter-layer features and soft label distillation. The inter-layer features from the GCN teacher network are converted into spike-form representations via the FTM, ensuring alignment with the spiking domain and facilitating the training of the SNN student network. Soft labels produced by the teacher network provide supplementary supervisory signals, optimizing the learning process. The subsequent sections provide a detailed description of the design and functionality of the modules.

3.2. Spiking Coding Mechanism and Spiking Multimodal Fusion

This chapter discusses how to convert continuous real skeleton data into spiking-form representation. Then, we describe how to effectively fuse the multimodal spike-form features derived from multimodal skeleton data.

3.2.1. Skeleton Spiking Coding Module

For a given 3D skeleton sequence data $X_i \in \mathbb{R}^{C \times T \times V}$, the SSC Module first transforms it into an image-like representation. Then it expands it into a form suitable for spiking temporal representation illustrated in Figure 2(a). The process is

described as follows:

$$P_0 = \text{Expand}(X_i) \in \mathbb{R}^{S \times C \times V \times T}, \quad (3)$$

$$P_i = \text{SN}(\text{BN}(\text{Conv2d}(P_0))) \in \mathbb{R}^{S \times N \times V \times T}. \quad (4)$$

In the initial step, the skeleton sequence data is transformed into an image-like representation to facilitate the structured feature extraction of spatial and temporal characteristics in subsequent stages. Subsequently, the $\text{Expand}(\cdot)$ operation adds a spike time step dimension to the data, reorganizing the temporal structure to align with the requirements of spiking representation. The resulting expanded representation P_0 incorporates the additional spike time step dimension S while preserving the original temporal dimension T , the graph structure V , and the channel size C .

Following expansion, the representation P_0 is processed through a 2D convolutional layer (Conv2d) with a kernel size of 3, followed by Batch Normalization (BN) and a Spiking Neuron (SN) layer. The pipeline refines the temporal-spatial features within the spiking domain, yielding a spiking feature representation P with dimensions $S \times N \times V \times T$. The spike time step dimension S captures the temporal structure of spiking activity, while the dimension T retains the temporal characteristics of the original sequence, ensuring a comprehensive temporal-spatial representation.

3.2.2. Spike-based Multimodal Fusion Module

Multimodal skeleton data consists of four components: bones (X_B), joints (X_J), bone motions (X_{BM}), and joint motions (X_{JM}), each represented with dimensions (C, T, V) .

The SMF module is a mutual information-based fusion framework formulated specifically for the sparse spike-form features derived from multimodal data. In the SMF, the multimodal skeleton data are first encoded independently through the SSC module to obtain their respective spike-form features: $P_B, P_J, P_{BM}, P_{JM} \in \mathbb{R}^{S \times D \times V \times T}$.

The spike-form features are then pairwise selected and concatenated along the feature dimension D to construct a joint distribution. To construct a corresponding marginal distribution, one of the two spike-form features in each pair is randomly shuffled along the spike time step dimension S , and the same concatenation is performed. We propose the Spike-form Mutual Information Calculation (SMIC) network, formally constituted by an LSTM network, SN, FC, and GAP layers, to realize the spiking-driven mutual information prediction. The framework computes the mutual information between four sparse spike-form features and performs weighted fusion. By leveraging the computational efficiency of sparse spike-form features and maximizing the lower bound of mutual information, the SMIC network effectively captures shared information across modalities, facilitating both robust and energy-efficient multimodal feature fusion within SNN framework, as illustrated in Figure 3b.

To illustrate the process, we take bone (P_B) and joint (P_J) data as an example. First, the spike-form features from the two modalities are concatenated along the feature dimension to con-

struct a joint distribution:

$$P_{\text{Joint}} = \text{cat}(P_J, P_B, \text{dim} = 1) \in \mathbb{R}^{S \times 2D \times V \times T}. \quad (5)$$

To generate a marginal distribution, the spike-form feature P_B is shuffled randomly along the spike time step dimension (S), resulting in P'_B . The shuffled feature is then concatenated with P_J :

$$P_{\text{marginal}} = \text{cat}(P_J, P'_B, \text{dim} = 1) \in \mathbb{R}^{S \times 2D \times V \times T}. \quad (6)$$

Both P_{Joint} and P_{marginal} are then processed through an LSTM network equipped with SN layers. For the joint distribution, the output of the LSTM is passed through a FC layer followed by a GAP operation to compute:

$$\mathbf{t}_1 = \text{SN}(\text{LSTM}(P_{\text{Joint}})), \quad \mathbf{t} = \text{GAP}(\text{FC}(\mathbf{t}_1)). \quad (7)$$

Similarly, for the marginal distribution, the output is processed through the same layers, and an additional exponential operation is applied:

$$\mathbf{et}_1 = \text{SN}(\text{LSTM}(P_{\text{marginal}})), \quad \mathbf{et} = \exp(\text{GAP}(\text{FC}(\mathbf{et}_1))). \quad (8)$$

Using the predictions \mathbf{t} and \mathbf{et} , the lower bound of mutual information is estimated as:

$$mi_lb = \bar{\mathbf{t}} - \log \bar{\mathbf{et}}. \quad (9)$$

The calculation is performed pairwise for all modalities—bones, joints, bone motions, and joint motions—resulting in six pairwise mutual information values, which are organized into a symmetric matrix \mathbf{MI} with zeros along the diagonal:

$$\mathbf{MI} = \begin{bmatrix} 0 & \cdots & mi_lb_{jb} \\ \vdots & \ddots & \vdots \\ mi_lb_{bj} & \cdots & 0 \end{bmatrix}_{4 \times 4}. \quad (10)$$

To normalize the mutual information values, the sum along the rows of \mathbf{MI} is computed, yielding the average mutual information weights:

$$\overline{\mathbf{MI}} = \frac{\sum_{i=1}^4 \mathbf{MI}_{i,:}}{\sum_{i=1}^4 \sum_{j=1}^4 \mathbf{MI}_{i,j}}, \quad (11)$$

$$\mathbf{W} = \frac{\overline{\mathbf{MI}} - \min(\overline{\mathbf{MI}})}{\max(\overline{\mathbf{MI}}) - \min(\overline{\mathbf{MI}})} \in \mathbb{R}^4. \quad (12)$$

The fused spike-form features are then obtained by weighting the original features of all modalities using \mathbf{W} :

$$P_{\text{fuse}} = \mathbf{W} * [P_B, P_J, P_{\text{BM}}, P_{\text{JM}}]^T \in \mathbb{R}^{S \times D \times V \times T}. \quad (13)$$

Finally, the fused feature P_{fuse} is fed into SGN Block for subsequent processing. By leveraging spiking-driven mutual information, the SMF module ensures the effective integration of sparse multimodal features, enhancing the robustness and accuracy of the overall action recognition framework.

3.3. SGN Block

Revisiting vanilla skeleton-based action recognition based on GCN, we construct our SGN using features converted into spike-form and adjacency matrices. The process can be summarized as follows:

$$S = \widetilde{D}^{-\frac{1}{2}} \widetilde{A} \widetilde{D}^{-\frac{1}{2}}, \quad (14)$$

where S is the normalized adjacency matrix, $\widetilde{A} = A + I$ denotes the sum of the adjacency matrix A and the identity matrix I (representing self-connections). \widetilde{D} is the diagonal degree matrix of A . The graph convolutional output is then calculated using the following formula:

$$H = S^K P \in \mathbb{R}^{S \times N \times T \times V}, \quad (15)$$

where, H represents the output of the early spatial spiking graph convolution, K is the number of graph convolutional layers, and P is the spike-form feature input. The first layer of SGC can be expressed as:

$$H^{(0)} = \text{SN}(P) + \text{SN}(H W_{\text{sgc}}^{(0)}), \quad (16)$$

where $W_{\text{sgc}}^{(0)} \in \mathbb{R}^{N^{(0)} \times N^{(1)}}$ is the learnable weight matrix of the first layer. Each subsequent layer has its learnable weights, denoted as $W_{\text{sgc}}^{(l)} \in \mathbb{R}^{N^{(l)} \times N^{(l+1)}}$.

To further enhance the model's representation capabilities, we incorporate Self Spiking Attention (SSA) following the principles of existing spiking attention methods. These methods leverage a spiking-based QKV structure with scaling factors s to control large matrix multiplication values. The computation of SSA can be described as follows:

$$Q^{(0)} = \text{SN}_Q(\text{BN}(H_0 W_Q^{(0)})), \quad (17)$$

$$K^{(0)} = \text{SN}_K(\text{BN}(H_0 W_K^{(0)})), \quad (18)$$

$$V^{(0)} = \text{SN}_V(\text{BN}(H_0 W_V^{(0)})), \quad (19)$$

$$H_{\text{SA}}^{(0)} = H_0 + \text{SN}\left(\left(Q^{(0)} K^{(0)T}\right) V^{(0)} \cdot s\right), \quad (20)$$

where, $Q^{(0)}$, $K^{(0)}$, and $V^{(0)}$ are computed through spiking neurons (SN) after Batch Normalization (BN) and linear transformations using learnable weights $W_Q^{(0)}$, $W_K^{(0)}$, and $W_V^{(0)}$. The attention mechanism integrates the weighted interactions, while the scaling factor s prevents large values in the spiking attention computation. $H_{\text{SA}}^{(0)}$ combines the residual connection H_0 with the attention-enhanced feature, defined as SA-SGC, illustrated in Figure 2(b), yielding a robust representation for spiking graph processing. After that, the first layer of STC can be written as:

$$T^{(0)} = \text{SN}\left(\text{BN}\left(\text{Conv2d}\left(H_{\text{SA}}^{(0)}\right)\right)\right) + \text{SN}\left(H_{\text{SA}}^{(0)}\right). \quad (21)$$

For subsequent layers, the spiking self attention-enhanced feature $H_{\text{SA}}^{(l)}$ is updated and combined with temporal features T^{l-1} ,

expressed as, illustrated in Figure 2(c):

$$H_{SA}^{(l)} = \text{SN}\left(T^{(l-1)}\right) + \text{SN}\left(H_{SA}^{(l-1)}W_{sgc}^{(l-1)}\right), \quad (22)$$

$$T^{(l)} = \text{SN}\left(\text{BN}^{(l)}\left(\text{Conv2d}^{(l)}\left(H_{SA}^{(l)}\right)\right)\right) + \text{SN}\left(H_{SA}^{(l)}\right). \quad (23)$$

Finally, the processed features are sent through GAP and a FC layer to output the prediction, as follows:

$$y = \text{FC}\left(\text{GAP}\left(\text{SN}\left(T^{(l)}\right)\right)\right), \quad (24)$$

where $y \in \mathbb{R}^U$, and U is the number of action classes. Based on this, a standard cross-entropy loss is adopted for model optimization, formulated as:

$$L_{\text{task}} = -\frac{1}{B} \sum_{b=1}^B \sum_{u=1}^U Y_{bu} \log y_{bu} + (1 - Y_{bu}) \log (1 - y_{bu}), \quad (25)$$

where, Y is the ground-truth label, y is the predicted output, and B denotes the number of training samples.

3.4. Knowledge Distillation of GCN-to-SGN

To leverage the powerful representation capabilities of multimodal GCNs, we propose a novel distillation framework with the multimodal GCN serving as the teacher network and the SGN as the student network, shown in Figure 4.

The proposed approach fully exploits the rich knowledge embedded in pre-trained multimodal GCNs, transferring superior representational features to the SGN. By aligning the intermediate features and outputs of the SGN with those of the GCN, shown in Figure 4a, the method significantly enhances SGN accuracy. The enhancement is achieved without introducing additional computational complexity or energy consumption, thereby preserving the inherent efficiency advantages of the SGN architecture. The distillation framework bridges the performance gap between GCNs and SGNs while maintaining the suitability of SGNs for energy-efficient applications.

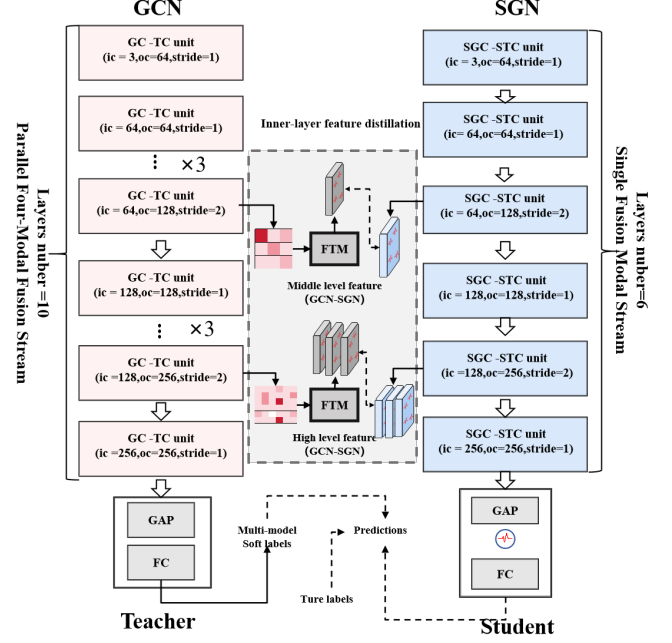
3.4.1. Soft Label Distillation

In the proposed distillation framework, the CTR-GCN with a 4-stream architecture is utilized as the teacher network. Multimodal data inputs, including bone, joint, bone-motion, and joint-motion data, are processed independently by single-stream CTR-GCN. Single-modal soft labels, represented as y_b , y_j , y_{bm} , and y_{jm} , are generated corresponding to the respective modalities.

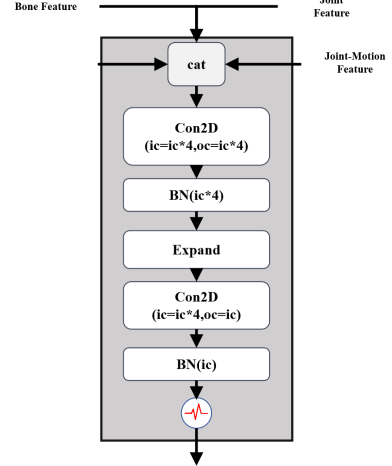
The outputs of the four modalities are then aggregated to form the multimodal soft labels \hat{y} , which serve as the knowledge to be distilled into the SGN. This aggregation is performed using weighted summation, as described below:

$$\hat{y} = \alpha_b y_b + \alpha_j y_j + \alpha_{bm} y_{bm} + \alpha_{jm} y_{jm}, \quad (26)$$

where α_b , α_j , α_{bm} , and α_{jm} are hyperparameters that control the relative contribution of each modality. These parameters are set based on the importance or reliability of the modalities during training.



(a) Inner-layer feature distillation and soft label distillation.



(b) The detail structure of FTM

Figure 4: GCN-to-SGN Knowledge Distillation Method

The SGN then learns to approximate the multimodal teacher soft labels \hat{y} through a regression-based loss function. The final learning objective for soft label distillation is expressed as:

$$L_{sdl} = \|y - \hat{y}\|, \quad (27)$$

where y represents the predictions of the SGN. By aligning its outputs with the teacher's multimodal soft labels, the SGN inherits the representational power of the multimodal GCN, improving its performance without increasing its energy consumption or computational cost.

3.4.2. Inner-layer feature distillation

The inner-layer features of heterogeneous GCN and SGN models differ significantly. While GCN typically processes continuous decimal values, SGN operates on sparse discrete

spike sequences. To address this discrepancy, we propose the FTM, as illustrated in Figure 4b. The FTM is an learnable module that transforms the continuous intermediate features of GCN into spike-form features, making them compatible with SGN.

The FTM concatenates multimodal features along the channel dimension and fuses them using depth-wise separable convolution. Subsequently, continuous features are expanded. Finally, spike-form features are generated through Conv2D, BN, and SN layers, ensuring compatibility between the teacher GCN and student SGN architectures while preserving the valuable structural and semantic information embedded in the GCN features.

In our distillation framework, the teacher GCN is composed of 10 GC-TC (Graph Convolution-Temporal Convolution) units, while the student SGN consists of 10 SGC-STC (Spiking Graph Convolution-Spiking Temporal Convolution) units. For feature distillation, we leverage intermediate-level features ($T_{Ab5}, T_{Aj5}, T_{Abm5}, T_{Ajm5}$) and high-level features ($T_{Ab8}, T_{Aj8}, T_{Abm8}, T_{Ajm8}$). The intermediate features are represented as: $T_{Ab5}, T_{Aj5}, T_{Abm5}, T_{Ajm5} \in \mathbb{R}^{2C \times \frac{T}{2} \times V}$, while the high-level features are: $T_{Ab8}, T_{Aj8}, T_{Abm8}, T_{Ajm8} \in \mathbb{R}^{4C \times \frac{T}{4} \times V}$. These layers are selected because the expansion of channel dimensions and the changes in stride within the TCN network allow them to capture diverse temporal relationships and richer feature information. Taking the intermediate 5th layer as an example, the multimodal teacher features are first concatenated and fused as follows:

$$T_{Am5} = \text{BN} \left(\text{Conv2D} \left(\text{cat} \left(T_{Ab5}, T_{Aj5}, T_{Abm5}, T_{Ajm5} \right) \right) \right), \quad (28)$$

where $T_{Am5} \in \mathbb{R}^{8C \times \frac{T}{2} \times V}$ represents the fused multimodal teacher features. These features are then translated into spike-form features through the FTM:

$$T_{Sm5} = \text{SN} \left(\text{BN} \left(\text{Conv2D} \left(\text{Expand} \left(T_{Am5} \right) \right) \right) \right), \quad (29)$$

where $T_{Sm5} \in \mathbb{R}^{S \times D \times V \times \frac{T}{2}}$ are the spike-form features. Similarly, the spike-form features for the high-level 8th layer (T_{Sm8}) are calculated.

To align the student SGN features with the teacher GCN features, we use cosine similarity as the loss function. For the intermediate 5th-layer spike-form feature and the corresponding SGN 3rd-layer spike-form feature (S_3), the loss is defined as:

$$L_{\text{fkd}_1} = \frac{1}{J} \sum_{j=1}^J \left(1 - \frac{T_{Sm5}^j \cdot S_3^j}{\|T_{Sm5}^j\| \cdot \|S_3^j\|} \right), \quad (30)$$

where J is the number of samples. Similarly, for the high-level 8th-layer spike-form feature and the SGN 5th-layer feature (S_5):

$$L_{\text{fkd}_2} = \frac{1}{J} \sum_{j=1}^J \left(1 - \frac{T_{Sm8}^j \cdot S_5^j}{\|T_{Sm8}^j\| \cdot \|S_5^j\|} \right). \quad (31)$$

Table 1: The details of the datasets used in our experiments.

Dataset	# Classes	Split				# Joints
		Cross-Subject		Cross-View (CSet)		
		# Train	# Test	# Train	# Test	
NTU RGB+D	60	40,320	16,560	37,920	18,960	25
NTU RGB+D 120	120	63,026	53,370	54,471	61,925	25
NW-UCLA	10	-	-	1,039	455	20

The inner-layer feature distillation loss is then defined as:

$$L_{\text{fkd}} = \beta_1 L_{\text{fkd}_1} + \beta_2 L_{\text{fkd}_2}, \quad (32)$$

where β_1 and β_2 are hyperparameters that control the weighting of the intermediate and high-level distillation losses. This formulation ensures that the student network effectively learns from the teacher’s intermediate and high-level spike-form features while optimizing the FTM for feature translation.

Finally, the overall learning objective combines the inner-layer feature distillation loss with the task loss L_{task} and the soft label distillation loss L_{sdk} as follows:

$$L = \gamma_1 L_b + \gamma_2 L_{\text{sdk}} + \gamma_3 L_{\text{fkd}}, \quad (33)$$

where γ_1 , γ_2 , and γ_3 are hyperparameters that balance the contribution of each loss term. This unified objective ensures that the SGN effectively inherits the representational power of the GCN while maintaining its energy efficiency and computational advantages.

4. Experiments

In this chapter, we present the implementation details, ablation studies, result comparisons, and visualizations, respectively. The details will be described in the following subsections.

4.1. Experimental Setup

4.1.1. Datasets

We evaluate the proposed method on three widely used skeleton-based action recognition datasets: NTU-RGB+D, NTU-RGB+D 120, and NW-UCLA[52, 53, 54]. These datasets provide diverse action classes, extensive skeleton data, and varying levels of complexity, making them ideal benchmarks for comprehensive evaluation.

NTU-RGB+D is a large-scale dataset comprising 60 action classes and 56,000 video clips. It includes detailed skeleton data covering a wide range of daily activities, captured using a Kinect v2 sensor. The dataset provides 3D coordinates of 25 major body joints, enabling precise modeling of human movements. NTU-RGB+D is widely recognized as a standard benchmark in the action recognition field due to its variety of actions and large-scale data volume. The dataset is evaluated under two standard settings: Cross-Subject (CSub), where training and testing samples are divided based on the subjects performing the actions, and Cross-View (CView), where training and testing samples are divided based on the camera views.

NTU-RGB+D 120, an extended version of NTU-RGB+D, significantly expands the dataset to include 120 action classes

Table 2: Hyperparameter settings for the LIF model.

Parameter	Value
Threshold V_{th}	1.0
Reset potential V_{reset}	0
Decay factor τ	0.25
Surrogate function’s window size a	1.0

and over 114,000 video clips. This dataset offers richer skeleton data, making it one of the largest and most comprehensive resources for skeleton-based action recognition. Its inclusion of a broader range of actions and more extensive data volume provides an ideal foundation for developing and evaluating advanced action recognition algorithms. Similarly, this dataset is evaluated under two standard settings: Cross-Subject (CSub) and Cross-Setup (CSet), where training and testing samples are divided based on the camera setups used during data collection.

NW-UCLA is a smaller dataset consisting of 10 action classes and 1,494 video clips captured from multiple viewpoints. It provides 3D coordinates of 20 major body joints, offering diverse skeleton data for assessing the robustness of action recognition models to viewpoint variations. The dataset poses a challenge for models to perform consistently across different perspectives. The evaluation is conducted under the Cross-View setting, where training and testing samples are divided based on the camera angles used for data capture.

The specific statistics for the three datasets after the splits are summarized in Table 1.

4.1.2. Implementation Details

The experiments are conducted on a server equipped with an NVIDIA SMI V100 GPU with 30 GB of memory. The models are implemented using PyTorch[56] and SpikingJelly[55], which provide efficient frameworks for spiking neural networks. During training, we use two separate SGD optimizers: one dedicated to optimizing the SGN model and the other specifically designed to refine the FTM. This dual-optimizer strategy enhances the efficiency of the SGN and ensures effective feature transfer from the teacher to the student model.

The key hyperparameters for the LIF model used in all experiments are listed in Table 2. The training configurations for MK-SGN across different datasets are summarized in Table 3. Additionally, Table 4 details the hyperparameters for soft label aggregation and loss weighting, including the weights assigned to different modalities ($\alpha_b, \alpha_j, \alpha_{bm}, \alpha_{jm}$) and the balancing factors for various loss components ($\beta_1, \beta_2, \gamma_1, \gamma_2, \gamma_3$).

The training configurations for MK-SGN across different datasets are summarized in Table 3. We adopt an initial learning rate of 0.1, a weight decay rate of 1e-4, and set the batch size based on the dataset: 64 for NTU-RGB+D 60, 32 for NTU-RGB+D 120, and 128 for NW-UCLA. Training is conducted for 64 epochs with a step decay schedule, reducing the learning rate after 50 epochs.

In the testing phase, only the SGN model is evaluated, isolating it from the dual-optimizer framework used during training. This ensures that the SGN’s performance reflects its learned ca-

Table 3: Hyperparameter settings for MK-SGN training.

Parameter	NTU-RGB+D	NTU-RGB+D	NW-UCLA
	60	120	
Learning Rate	0.1/0.1	0.1/0.1	0.1/0.1
Decay Rate	0.1/0.1	0.1/0.1	0.1/0.1
Batch Size	64	32	128
Time Steps	4	4	4
Training Epochs	64	64	64
Step	50	50	50
Dropout Rate	0.3	0.3	0.3
Weight Decay	1e-4	1e-4	1e-4
Optimizer	SGD/SGD	SGD/SGD	SGD/SGD

Table 4: Hyperparameters for soft label aggregation and loss weighting.

Hyperparameter	Description	Value
α_b	Weight for bone modality.	0.25
α_j	Weight for joint modality.	0.25
α_{bm}	Weight for bone motion modality.	0.25
α_{jm}	Weight for joint motion modality.	0.25
β_1	Weight of intermediate distillation loss.	0.5
β_2	Weight of high-level distillation loss.	0.5
γ_1	Weight of task loss term.	1.0
γ_2	Weight of soft label loss term.	1.0
γ_3	Weight of feature distillation loss term.	1.0

pabilities without additional computational overhead.

4.2. Ablation Studies

To verify the effectiveness and efficiency of the proposed model, we first replace the activation layers of the classic one-stream 2S-AGCN model with LIF neurons. This modified model, called Base-SGN*, is then trained and tested for comparison. Additionally, we compare our proposed model with Spikformer, a classic SNN-based transformer architecture. For a fair comparison, we adjust the layer structure and hidden dimension of Spikformer to match the MK-SGN architecture. These adjustments ensure that the comparison focuses on the modeling approach while minimizing the influence of structural differences. Based on these baselines, we conduct ablation and comparison experiments to evaluate the performance of MK-SGN.

4.2.1. Theoretical Energy Consumption Calculation

In the context of SNNs, synaptic operations (SOPs) play a critical role in determining theoretical energy consumption. As one of the key components of our experimental evaluation, we focus on calculating SOPs and the energy consumption of both Base-SGN* and MK-SGN, highlighting the efficiency of the proposed model.

Following [27, 28, 29], the firing rate r of each LIF neuron, is defined as the firing probability per spike time step. Using the firing rate r , the synaptic operations for a given block or layer l are expressed as:

$$\text{SOPs}(l) = r \times S \times \text{FLOPs}(l), \quad (34)$$

where $\text{FLOPs}(l)$ refers to the floating-point operations of l , defined as the number of multiply-and-accumulate(MAC) opera-

Table 5: Evaluation on NTU-RGB+D. Param refers to the number of parameters. Power is the average theoretical energy consumption when predicting a skeleton from the NTU-RGB+D test set, whose calculation details are shown in Equation(35), Equation(36), and Equation(37).

Method	Architecture	Param (M)	Spike Time Step	SMF	Knowledge Distillation	SOPs (G)	FLOPs (G)	Power (mJ)	Ntu-RGB+D 60	
									CSub(%)	CView(%)
ANN	(10-layer)ST-GCN	3.1	/	/	/	/	3.48	16.01	81.5	88.3
SNN	(10-layer)Base-SGN*	2.07	4	/	/	0.60	7.17	0.536	64.2	71.3
	(6-layer)Spikformer ^{ICLR 2023}	4.78	4	/	/	1.69	24.07	2.17	73.9	80.6
	(6-layer) MK-SGN	1.89	4	/	/	0.64	7.32	0.573	74.5	80.9
	(6-layer) MK-SGN	1.89	4	/	✓	0.66	7.32	0.582	75.9	82.1
	(6-layer) MK-SGN	2.17	4	✓	/	0.67	7.76	0.596	76.1	82.6
	(6-layer) MK-SGN	2.17	4	✓	✓	0.68	7.76	0.614	78.5	85.6

Note: FLOPs are calculated using the FVCORE library, which provides precise computation of floating-point operations.

tions performed in l block or layer. And SOPs are the number of spike-based accumulate (AC) operations.

The theoretical energy consumption of Base-SGN and MK-SGN is calculated as follows:

$$E_{\text{Base-SGN}} = E_{\text{MAC}} \times \text{FL}_{\text{SNNConv}}^1 + E_{\text{AC}} \times \left(\sum_{n=2}^N \text{SOP}_{\text{SNNConv}}^n + \sum_{m=1}^M \text{SOP}_{\text{SNNFC}}^m \right), \quad (35)$$

$$E_{\text{MK-SGN}} = n_m \times E_{\text{MAC}} \times \text{FL}_{\text{SNNConv}}^1 + E_{\text{AC}} \times \left(\frac{k \times (k-1)}{2} \text{SOP}_{\text{SMIC}} + \sum_{n=n_m}^N \text{SOP}_{\text{SNNConv}}^n + \sum_{m=1}^M \text{SOP}_{\text{SNNFC}}^m + \sum_{l=1}^L \text{SOP}_{\text{SSA}}^l \right). \quad (36)$$

In these equations, $\text{FL}_{\text{SNNConv}}^1$ represents the initial layer responsible for encoding skeleton data into spike-form, while SOP_{SMIC} accounts for the energy cost of modality fusion with k denoting the number of modalities.

Energy consumption is estimated under the assumption of 45nm hardware, with $E_{\text{MAC}} = 4.6 \text{ pJ}$ and $E_{\text{AC}} = 0.9 \text{ pJ}$ [57]. The power consumption for a block b in ANN (MAC-based) and SNN (SOP-based) frameworks is given by:

$$\text{Power}(b) = 4.6 \text{ pJ} \times \text{FLOPs}(b), \quad (37)$$

$$\text{Power}(b) = 0.9 \text{ pJ} \times \text{SOPs}(b). \quad (38)$$

These formulations demonstrate how MK-SGN balances high performance with reduced theoretical energy consumption. SOPs, representing synaptic operations, serve as a critical metric for evaluating the energy efficiency of spiking-driven architectures.

4.2.2. The Effect of Different Components

To analyze the energy efficiency of the proposed MK-SGN and evaluate the contribution of each component within the model, we use theoretical formulas to estimate the number of operations(OPs) required for classifying a single action sample. Specifically, we calculate the FLOPs for ANN-based models, as well as the FLOPs for SNN on traditional GPUs and the theoretical SOPs on neuromorphic hardware. Using these operation counts, we further compute the energy consumption per action

Table 6: Performance comparison for different modality combinations using the SMF module. Accuracy is tested on Ntu-RGB+D Xsub

Architecture	Modalities	Parameters	Ops	Power	Accuracy
		(M)	(G)	(mJ)	(%)
MK-SGN	J	1.89	0.64	0.573	74.5
	J+B	1.98	0.65	0.584	75.6
	J+B+JM	2.08	0.66	0.591	75.9
	J+B+JM+BM	2.17	0.67	0.596	76.1

sample during the testing phase.

Additionally, we evaluate the classification accuracy of MK-SGN through comprehensive ablation studies conducted on the NTU-RGB+D 60 dataset. The results, including energy efficiency and accuracy comparisons, are summarized in Table 5.

Base-SGN*. First, we validate the effectiveness of Base-SGN* as the foundation for the ablation study. We use the trained model and compare it with the vanilla ST-GCN. We calculate the theoretical number of OPs and energy consumption. The results show that Base-SGN* reduces the theoretical energy consumption by 0.536 mJ per action sample. However, this increases the FLOPs and decreases the accuracy to 64.2% and 71.3%. This indicates that simply replacing the activation layer is insufficient to maintain high classification accuracy.

MK-SGN. Building on Base-SGN*, we compare its performance with the proposed MK-SGN. Even without knowledge distillation, the single-modality MK-SGN achieves significant accuracy improvements of 10.1% and 8.9% on XSub and XView settings, respectively, with only a minimal increase in OPs and theoretical power consumption. Compared to ST-GCN, although MK-SGN demonstrates a slight increase in FLOPs, this trade-off is offset by its extremely low SOPs value of 0.68, which highlights its suitability for deployment on neuromorphic hardware. Furthermore, MK-SGN reduces the parameter count by over 50% and decreases FLOPs and theoretical energy consumption by more than 70% compared to structurally similar models like Spikformer, while maintaining competitive computational efficiency. Furthermore, MK-SGN achieves an accuracy improvement of 0.6% on XSub and 0.3% on XView compared to Spikformer, demonstrating its superior balance of performance and efficiency. These results highlight the effectiveness of MK-SGN in achieving high accuracy with significantly reduced computational and energy requirements.

Table 7: Accuracy comparison under different knowledge distillation settings. Accuracy is tested on Ntu-RGB+D Xsub

Setting	SKD	IFD	Modalities	Accuracy (%)
-	-	-	-	74.5
Soft Label Only	✓	-	J	75.1
Soft Label (Two Modal.)	✓	-	J+B	75.4
Soft Label (Four Modal.)	✓	-	J+B+JM+BM	75.6
Inner-layer (Low)	-	✓	J+B+JM+BM	74.9
Inner-layer (High)	-	✓	J+B+JM+BM	75.3
Full KD	✓	✓	J+B+JM+BM	75.9

SMF. In the case of late fusion in a multi-modal classification network, where n_n represents the number of modalities, classifying a single action sample requires n_n independent testing runs. This leads to a theoretical energy consumption scaled by n_n times. Taking ST-GCN as an example, its theoretical OPs will become 4×3.48 G, and the Power will increase to 4×16.01 mJ.

To validate the effectiveness of the designed SMF module in avoiding the increased energy consumption caused by late fusion while simultaneously improving accuracy, we conduct more in-depth experiments, as shown in Table 6. Specifically, we incrementally integrate different modalities such as Joint (J), Joint+Bone (J+B), Joint+Bone+Joint-Motion (J+B+JM) and Joint+Bone+Joint-Motion +Bone-Motion(J+B+JM+BM)

The results demonstrate the effectiveness of the SMF module in achieving a balanced trade-off between energy efficiency and classification accuracy. For single modal, the model achieves an accuracy of 74.5% with a theoretical power consumption of 0.573 mJ. As additional modalities are integrated, the accuracy steadily increases, reaching 76.1% for the full multimodal fusion (J+B+JM+BM). Notably, the increase in accuracy is achieved with only a minimal increase in theoretical energy consumption, which rises from 0.573 mJ for single-modality fusion to 0.596 mJ for four modalities.

The number of parameters also exhibits a controlled increase, growing from 1.89 M for single-modal fusion to 2.17 M for multimodal fusion, demonstrating the efficiency of the SMF module in leveraging additional modalities without significantly increasing model complexity. The theoretical OPs follow a similar trend, incrementally rising from 0.64 G to 0.67 G.

These results validate that the SMF module effectively avoids the exponential increase in energy consumption caused by late fusion while consistently improving accuracy. Compared to single-modality fusion, the full multimodal fusion achieves an improvement of 1.6% in accuracy for CSub, showcasing the robustness of the SMF module in efficiently integrating information across multiple modalities. This balance of efficiency and accuracy highlights the superiority of SMF over traditional late fusion methods.

Knowledge Distillation of GCN-to-SGN. We compare the accuracy of SGN models trained with and without teacher guidance to evaluate the impact of our proposed knowledge distillation method. Knowledge distillation consists of two components: soft label distillation (SKD) and inner-layer feature distillation (IFD). To further analyze their contributions, we con-

duct experiments with and without each component. Additionally, we investigate the impact of soft label distillation using different modality combinations, as well as the effect of inner-layer feature distillation applied at different levels (low-level, high-level, or both).

The results in Table 7 demonstrate the significant contributions of SKD and IFD to the accuracy improvements of SGN models. With the introduction of SKD, accuracy improves steadily as more modalities are incorporated. Single-modality SKD achieves 75.1%, while combining two and four modalities further enhances the performance to 75.4% and 75.6%, respectively. This progression highlights the importance of multimodal knowledge transfer from the teacher network to the student model.

For IFD, focusing on low-level features yields an accuracy of 74.9%, while high-level features achieve 75.3%, indicating that the more abstract information encoded in high-level features plays a slightly greater role in guiding the student model. However, combining both low-level and high-level feature distillation demonstrates their complementary effects, achieving a final accuracy of 75.9% when combined with SKD in the full knowledge distillation (Full KD) setup.

The results highlight the importance of leveraging both output-level and feature-level guidance. While SKD aligns the student’s outputs with the teacher’s multimodal predictions, IFD bridges the gap in intermediate representations, allowing the student to better emulate the teacher’s internal structure. The findings validate the proposed knowledge distillation framework as an effective means of improving SGN model performance through both comprehensive guidance and multimodal integration.

Integrated Module Performance Comparison. We carefully evaluate the contributions of each component in the MK-SGN model, with results summarized in Table 5. The fully integrated MK-SGN achieves accuracies of 78.5% and 85.6% on XSub and XView settings, respectively, with a spike time step of 4. Compared to Spikformer, MK-SGN reduces the parameter count by 54.6% and FLOPs by 67.4%, significantly enhancing its feasibility for training on traditional GPUs. Moreover, MK-SGN decreases SOPs by 59.76% and theoretical energy consumption by 71.7%, while achieving accuracy improvements of 4.6% and 5.0%, demonstrating its ability to balance high performance with low energy consumption.

Compared to Base-SGN*, MK-SGN delivers substantial accuracy gains of 14.3% and 11.3% on XSub and XView, respectively. Additionally, when compared to the classic ANN-based model ST-GCN, MK-SGN achieves a remarkable 94.78% reduction in energy consumption while maintaining comparable accuracy. These results highlight the efficiency and effectiveness of MK-SGN, showcasing its suitability for energy-constrained applications without compromising performance.

4.3. Comparison with State-of-the-Art Methods

In this section, we conduct a comprehensive comparison between our proposed MK-SGN and SOTA methods for skeleton-based action recognition. The comparison is divided into two

parts:(1). model architecture comparison and (2).metric comparison.

In the model architecture comparison, we focus on the design and layer configurations of MK-SGN in contrast to GCN and SNN models, using the NTU-RGB+D 60 dataset as a case study. This includes both publicly available results and those we reproduced under consistent experimental settings. The architecture analysis establishes the foundation for understanding the computational and operational differences, which are crucial for fair metric comparisons.

In the metric comparison, we evaluate MK-SGN against SOTA models across several dimensions, including accuracy, number of operations (OPs), and theoretical energy consumption. These metrics provide a quantitative perspective on MK-SGN’s ability to balance high performance with energy efficiency, particularly in energy-constrained environments.

By integrating both structural and performance analyses, we aim to demonstrate the superiority of MK-SGN in achieving competitive results with significantly reduced energy and computational overhead, establishing its practicality and effectiveness in real-world applications.

4.3.1. Model Architecture Comparison

Table 8 summarizes the architectural differences between our proposed MK-SGN and various SOTA models, including GCN, and Spikformer, as applied to the NTU-RGB+D 60 dataset. This comparison highlights how each model is structured to handle skeleton-based action recognition tasks, with adaptations made to ensure fair performance evaluations.

The GCN model serves as a classical ANN-based approach, employing GC layers combined with TC layers for spatio-temporal feature extraction. Its structure consists of 10 layers of GC-TC operations, with progressively increasing feature dimensions and downsampling via strides, culminating in a GAP-FC layer for classification. This architecture represents a strong baseline for ANN-based recognition.

The Base-SGN* model acts as the baseline SNN structure, leveraging SGC and STC layers to process spike-form data. It follows a similar configuration to GCN but is adapted for spiking computation. However, it lacks the advanced features introduced in MK-SGN.

The Spikformer model, a spiking-based Transformer, incorporates SSA layers and MLP components for feature extraction. For this study, we modified Spikformer to align with MK-SGN in terms of layer count and hidden dimensions, ensuring a fair comparison of metrics such as energy efficiency and accuracy. This adjustment enables us to evaluate the performance of Spikformer in a setting directly comparable to MK-SGN. Similarly, other network variations like Spiking-driven-former, Spiking-driven-former v2 and Spiking Wavelet Transformer used in the study are adapted to maintain consistency across evaluations.

Finally, the MK-SGN model stands out with its innovative spiking-specific modules, including the SSC and SMF modules, which enhance multimodal integration and energy efficiency. The SGC-STC layers are optimized for spike-form data, enabling MK-SGN to balance high accuracy with reduced compu-

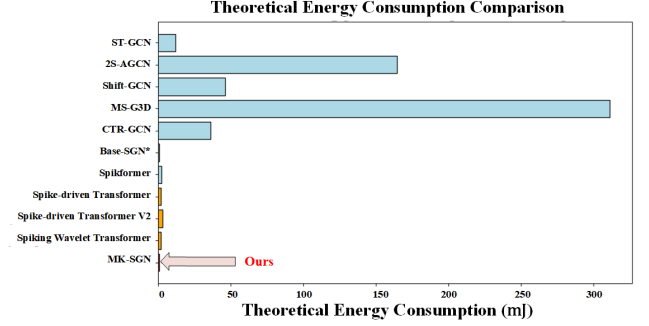


Figure 5: Theoretical Energy Consumption Comparison

tational and energy requirements, setting it apart as an advanced solution for real-world applications.

This architectural comparison provides the groundwork for the subsequent metric analysis, ensuring that the reproduced models are aligned in structure and settings to allow for fair and meaningful performance evaluations.

4.3.2. Metric Comparison

We compare our proposed MK-SGN with the current SOTA ANNs and SNNs in skeleton-based action recognition, focusing on two critical performance metrics: OPs and theoretical energy consumption. The results are summarized in Table 9 and Table 10.

To ensure fairness, the reported results for existing multi-modal GCN methods utilize all four modalities: joint, bone, joint motion, and bone motion. For these methods, the softmax scores of multiple streams are fused by summing the scores from each stream. The OPs and theoretical energy consumption for these multi-modal methods are calculated by multiplying the values for a single stream by the total number of modalities.

Additionally, we reproduce the results of SOTA SNN models using only the joint modality to provide a direct and fair comparison with MK-SGN. These reproduced SNN models are carefully adapted to align with MK-SGN in terms of the number of layers and hidden dimensions. This ensures consistency in the experimental settings and allows for a robust evaluation of their efficiency and effectiveness.

The comparison highlights that MK-SGN strikes a remarkable balance between accuracy and energy efficiency. Compared to existing methods, MK-SGN achieves significant reductions in theoretical energy consumption, emphasizing its suitability for energy-constrained scenarios, such as edge computing and real-time applications. By leveraging its spiking-driven architecture, MK-SGN demonstrates the ability to deliver competitive or superior performance while maintaining exceptional energy efficiency. Detailed results and analysis are provided in the following subsections.

Results on NTU-RGB+D 60 and 120. As shown in Table 9, MK-SGN demonstrates superior performance on both NTU-RGB+D 60 and NTU-RGB+D 120 datasets, showcasing its remarkable energy efficiency and competitive accuracy.

Table 8: Model’s architecture for NTU-RGB+D 60

Layer	GCN (Input/Output)	GCN Structure Layer Composition	Base-SGN (Input/Output)	MK-SGN (Input/Output)	SGN Structure Layer Composition	Spikformer (Input/Output)	Spikformer Structure Layer Composition
Fire layer	-	-	3/3	3/3	SC-(SMF)	3/256	SPS
1	3/64	GC-TC	3/64	3/64	SGC-STC	256/256	SSA-MLP
2	64/64	GC-TC	64/64	64/64	SGC-STC	256/256	SSA-MLP
3	64/64	GC-TC	64/64	64/128(stride=2)	SGC-STC	256/256	SSA-MLP
4	64/64	GC-TC	64/64	128/128	SGC-STC	256/256	SSA-MLP
5	64/128(stride=2)	GC-TC	64/128(stride=2)	128/256(stride=2)	SGC-STC	256/256	SSA-MLP
6	128/128	GC-TC	128/128	256/256	SGC-STC	256/256	SSA-MLP
7	128/128	GC-TC	128/128	-	SGC-STC	-	-
8	128/256(stride=2)	GC-TC	128/256(stride=2)	-	SGC-STC	-	-
9	256/256	GC-TC	256/256	-	SGC-STC	-	-
10	256/256	GC-TC	256/256	-	SGC-STC	-	-
final	256/class number	GAP-FC	256/class number	256/class number	GAP-SN-FC	256/class number	GAP-FC

Table 9: Comparative results on NTU RGB+D 60 and 120. We evaluate our model in terms of classification accuracy (%). X-Sub and X-View represent cross-subject and cross-view splits.

Method	Architecture	Backbone	Spike Time Step	Performance			Accuracy (%)			
				Param (M)	OPs (G)	Power (mJ)	Csub (60)	Cview (60)	Csub (120)	CSet (120)
Lie Group[58]	ANN	CNN	/	/	/	/	50.1	52.8	/	/
HBRNN [8]	ANN	RNN	/	/	/	/	59.1	64.0	/	/
Deep LSTM[52]	ANN	LSTM	/	/	/	/	60.7	67.3	/	/
ST-GCN [11]	ANN	GCN	/	3.1	3.48	16.01	81.5	88.3	70.7	73.2
2S-AGCN [12]	ANN	GCN	/	3.48	35.8	164.68	88.5	95.0	82.5	84.2
Shift-GCN [13]	ANN	GCN	/	/	10	46	90.7	96.5	85.9	87.6
MS-G3D [59]	ANN	GCN	/	3.19	67.63	311.09	91.5	96.2	86.9	88.4
CTR-GCN[14]	ANN	GCN	/	1.46	7.88	36.25	92.4	96.8	88.9	90.6
Base-SGN*	SNN	SGN	4	2.07	0.60	0.536	64.2	71.3	45.2	47.3
Spikformer[27] ^{ICLR 2023}	SNN	Spiking Transformer	4	4.78	1.69	2.17	73.9	80.1	61.7	63.7
Spike-driven Transformer[28] ^{NIPS2023}	SNN	Spiking Transformer	4	4.77	1.57	1.93	73.4	80.6	62.3	64.1
Spike-driven Transformer V2[29] ^{ICLR 2024}	SNN	Spiking Transformer	4	11.47	2.59	2.91	77.4	83.6	64.3	65.9
Spiking Wavelet Transformer[60] ^{ECCV 2025}	SNN	Spiking Transformer	4	3.24	1.48	2.01	74.7	81.2	63.5	64.7
MK-SGN (Ours)	SNN	SGN	4	2.17	0.68	0.614	78.5	85.6	67.8	69.5

Note: FLOPs are calculated using the FVCORE library, which provides precise computation of floating-point operations.

On the NTU-RGB+D 60 and NTU-RGB+D 120 datasets, MK-SGN achieves a significant reduction in theoretical energy consumption, requiring only 0.614 mJ per sample. This represents a **96.16%** decrease compared to ST-GCN (16.01 mJ), a **99.63%** decrease compared to 2S-AGCN (164.68 mJ), and a **99.80%** decrease compared to MS-G3D (311.09 mJ). Even when compared to lightweight models like Shift-GCN (46 mJ) and CTR-GCN (36.25 mJ), MK-SGN reduces energy consumption by **98.67%** and **98.31%**, respectively, highlighting its remarkable efficiency advantage across all ANN-based GCN architectures, as showed in Figure 5.

Beyond energy savings, MK-SGN surpasses SOTA SNN-based models in both accuracy and efficiency, as highlighted in Table 9 and Figure 6. For NTU-RGB+D 60, MK-SGN achieves classification accuracies of 78.5% (Csub) and 85.6% (Cview), outperforming competitive SNN models such as Spikformer (73.9% Csub, 80.1% Cview) and Spike-driven Transformer V2 (77.4% Csub, 83.6% Cview). Importantly, MK-SGN achieves this with significantly reduced energy consumption, requiring only 0.614 mJ per sample compared to Spikformer’s 2.17 mJ and Spike-driven Transformer V2’s 2.91 mJ. MK-SGN also demonstrates an efficient parameter design with 2.17M param-

eters, far less than Spike-driven Transformer V2’s 11.47M, highlighting its lightweight and efficient architecture.

On the NTU-RGB+D 120 dataset, MK-SGN continues to outperform SNN models, achieving accuracies of 67.8% (Csub) and 69.5% (CSet). In comparison, Spikformer achieves 61.7% (Csub) and 63.7% (CSet), while Spike-driven Transformer V2 achieves 64.3% (Csub) and 65.9% (CSet). Despite these improvements in accuracy, MK-SGN remains highly energy-efficient, consuming only 0.614 mJ, compared to Spiking Wavelet Transformer’s 2.01 mJ and Spike-driven Transformer V2’s 2.91 mJ. This demonstrates MK-SGN’s superior performance and efficiency across datasets.

These results validate MK-SGN as a robust and energy-efficient solution for skeleton-based action recognition, excelling in scenarios requiring both high accuracy and low computational cost. By leveraging its spiking-driven architecture, MK-SGN sets a new benchmark for balancing performance and efficiency in SNN.

Results on NW-UCLA. On the NW-UCLA dataset, as summarized in Table 10, MK-SGN achieves a classification accuracy of 92.3%, surpassing SOTA SNN models. It outperforms models like Spikformer (85.4%) and Spike-driven Transformer

Table 10: Comparative results on NW-UCLA. We evaluate our model in terms of classification accuracy (%).

Method	Architecture	Backbone	Times	Param. (M)	OPs (G)	Power (mJ)	Acc (%)
Lie Group[58]	ANN	CNN	/	-	-	-	74.2
Actionlet ensemble [61]	ANN	CNN	/	-	-	-	76.0
HBRNN-L[63]	ANN	RNN	/	-	-	-	78.5
Ensemble TS-LSTM [62]	ANN	LSTM	/	-	-	-	89.2
Shift-GCN [13]	ANN	GCN	/	-	0.7	3.22	94.6
CTR-GCN [14]	ANN	GCN	/	1.46	2.48	12.15	96.5
Base-SGN*	SNN	SGN	4	2.07	0.151	0.195	86.4
Spikformer[27] ^{ICLR 2023}	SNN	Spiking Transformer	4	4.78	0.513	0.673	85.4
Spike-driven Transformer[28] ^{NIPS2023}	SNN	Spiking Transformer	4	4.77	0.501	0.643	83.4
Spike-driven Transformer V2[29] ^{ICLR 2024}	SNN	Spiking Transformer	4	11.47	0.754	0.914	89.4
Spiking Wavelet Transformer[60] ^{ECCV 2025}	SNN	Spiking Transformer	4	3.24	0.451	0.697	86.9
MK-SGN (Ours)	SNN	SGN	4	2.17	0.165	0.207	92.3

Note: FLOPs are calculated using the FVCORE library, which provides precise computation of floating-point operations.

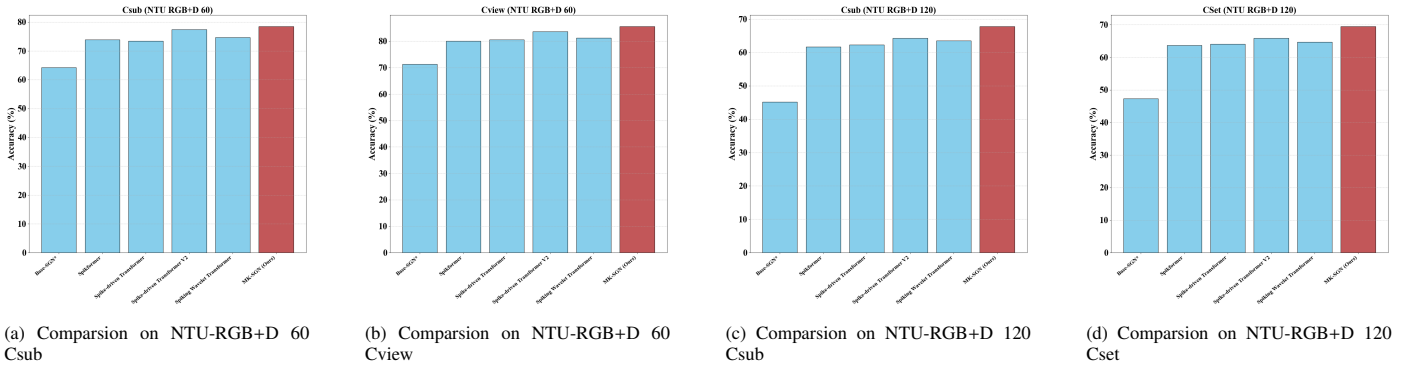


Figure 6: Comparison of Accuracy with SOTA SNN

V2 (89.4%) while maintaining significantly lower energy consumption, consuming only 0.207 mJ per sample compared to 0.914 mJ for Spike-driven Transformer V2.

This highlights MK-SGN’s ability to effectively balance accuracy and energy efficiency without compromising its computational performance. Its lightweight structure and optimized spiking modules allow for efficient recognition, particularly in scenarios where minimizing resource consumption is critical. These results further emphasize MK-SGN’s versatility and practicality across diverse application settings.

5. Conclusion

In this work, we propose the Spiking Graph Convolutional Network (MK-SGN), a novel architecture that combines the strengths of SNNs and graph convolutional networks GCNs for skeleton-based action recognition. This framework is, to the best of our knowledge, the first to effectively integrate spiking neural computation with graph-based modeling, offering a new perspective on energy-efficient and high-performance recognition methods.

The MK-SGN addresses the critical challenge of high energy consumption in traditional GCN-based methods while maintaining competitive performance. By leveraging multimodal fusion and knowledge distillation, MK-SGN not only optimizes the use of spiking neural computation but also enhances the ability to extract and integrate meaningful features across

modalities. These innovations enable MK-SGN to significantly reduce energy consumption on three benchmark skeleton action recognition datasets, achieving over 98% reduction compared to the best ANN-based methods.

Moreover, MK-SGN consistently surpasses SOTA SNN models in recognition accuracy, achieving an average improvement of 5%. This highlights its ability to balance energy efficiency and computational effectiveness, making it particularly well-suited for real-time and resource-constrained applications. These results establish MK-SGN as a robust and practical solution for skeleton-based action recognition, paving the way for future exploration of spiking-based multimodal frameworks in other domains.

References

- [1] H. B. Zhang, Y. X. Zhang, B. Zhong, Q. Lei, L. Yang, J. X. Du, and D. S. Chen, *A comprehensive survey of vision-based human action recognition methods*, *Sensors*, 19(5), 1005, 2019.
- [2] P. Khaire and P. Kumar, *Deep learning and RGB-D based human action, human-human and human-object interaction recognition: A survey*, *Journal of Visual Communication and Image Representation*, 86, 103531, 2022.
- [3] B. Ren, M. Liu, R. Ding, and H. Liu, *A survey on 3d skeleton-based action recognition using learning method*, *Cyborg and Bionic Systems*, 5, 0100, 2024.
- [4] K. Zhu, R. Wang, Q. Zhao, J. Cheng, and D. Tao, *A cuboid CNN model with an attention mechanism for skeleton-based action recognition*, *IEEE Transactions on Multimedia*, 22(11), 2977–2989, 2019.

- [5] Z. Ding, P. Wang, P. O. Ogunbona, and W. Li, *Investigation of different skeleton features for CNN-based 3D action recognition*, in *2017 IEEE International Conference on Multimedia & Expo Workshops (ICMEW)*, pp. 617–622, IEEE, July 2017.
- [6] B. Li, Y. Dai, X. Cheng, H. Chen, Y. Lin, and M. He, *Skeleton based action recognition using translation-scale invariant image mapping and multi-scale deep CNN*, in *2017 IEEE International Conference on Multimedia & Expo Workshops (ICMEW)*, pp. 601–604, IEEE, July 2017.
- [7] Y. Du, Y. Fu, and L. Wang, *Representation learning of temporal dynamics for skeleton-based action recognition*, *IEEE Transactions on Image Processing*, 25(7), 3010–3022, 2016.
- [8] Y. Du, W. Wang, and L. Wang, *Hierarchical recurrent neural network for skeleton-based action recognition*, in *Proceedings of the IEEE Conference on Computer Vision and Pattern Recognition*, pp. 1110–1118, 2015.
- [9] J. Liu, G. Wang, L. Y. Duan, K. Abdiyeva, and A. C. Kot, *Skeleton-based human action recognition with global context-aware attention LSTM networks*, *IEEE Transactions on Image Processing*, 27(4), 1586–1599, 2017.
- [10] T. Ahmad, L. Jin, X. Zhang, S. Lai, G. Tang, and L. Lin, *Graph convolutional neural network for human action recognition: A comprehensive survey*, *IEEE Transactions on Artificial Intelligence*, 2(2), 128–145, 2021.
- [11] S. Yan, Y. Xiong, and D. Lin, *Spatial temporal graph convolutional networks for skeleton-based action recognition*, in *Proceedings of the AAAI Conference on Artificial Intelligence*, Vol. 32, No. 1, April 2018.
- [12] L. Shi, Y. Zhang, J. Cheng, and H. Lu, *Two-stream adaptive graph convolutional networks for skeleton-based action recognition*, in *Proceedings of the IEEE/CVF Conference on Computer Vision and Pattern Recognition*, pp. 12026–12035, 2019.
- [13] K. Cheng, Y. Zhang, X. He, W. Chen, J. Cheng, and H. Lu, *Skeleton-based action recognition with shift graph convolutional network*, in *Proceedings of the IEEE/CVF Conference on Computer Vision and Pattern Recognition*, pp. 183–192, 2020.
- [14] Y. Chen, Z. Zhang, C. Yuan, B. Li, Y. Deng, and W. Hu, *Chamel-wise topology refinement graph convolution for skeleton-based action recognition*, in *Proceedings of the IEEE/CVF International Conference on Computer Vision*, pp. 13359–13368, 2021.
- [15] H. G. Chi, M. H. Ha, S. Chi, S. W. Lee, Q. Huang, and K. Ramani, *InfoGCN: Representation learning for human skeleton-based action recognition*, in *Proceedings of the IEEE/CVF Conference on Computer Vision and Pattern Recognition*, pp. 20186–20196, 2022.
- [16] Y. Wang, Y. Wu, S. Tang, W. He, X. Guo, F. Zhu, et al., *HULK: A universal knowledge translator for human-centric tasks*, *arXiv preprint arXiv:2312.01697*, 8, 2023.
- [17] A. Tavanaei, M. Ghodrati, S. R. Kheradpisheh, T. Masquelier, and A. Maida, *Deep learning in spiking neural networks*, *Neural Networks*, 111, 47–63, 2019.
- [18] K. Yamazaki, V. K. Vo-Ho, D. Bulsara, and N. Le, *Spiking neural networks and their applications: A review*, *Brain Sciences*, 12(7), 863, 2022.
- [19] F. Ponulak and A. Kasinski, *Introduction to spiking neural networks: Information processing, learning and applications*, *Acta Neurobiologicae Experimentalis*, 71(4), 409–433, 2011.
- [20] N. Rathhi, I. Chakraborty, A. Kosta, A. Sengupta, A. Ankit, P. Panda, and K. Roy, *Exploring neuromorphic computing based on spiking neural networks: Algorithms to hardware*, *ACM Computing Surveys*, 55(12), 1–49, 2023.
- [21] N. Yin, M. Wang, Z. Chen, G. De Masi, H. Xiong, and B. Gu, *Dynamic spiking graph neural networks*, in *Proceedings of the AAAI Conference on Artificial Intelligence*, Vol. 38, No. 15, pp. 16495–16503, March 2024.
- [22] H. Zhao, X. Yang, C. Deng, and J. Yan, *Dynamic Reactive Spiking Graph Neural Network*, in *Proceedings of the AAAI Conference on Artificial Intelligence*, Vol. 38, No. 15, pp. 16970–16978, March 2024.
- [23] Z. Zhu, J. Peng, J. Li, L. Chen, Q. Yu, and S. Luo, *Spiking graph convolutional networks*, *arXiv preprint arXiv:2205.02767*, 2022.
- [24] B. Yin, F. Corradi, and S. M. Bohtë, *Accurate and efficient time-domain classification with adaptive spiking recurrent neural networks*, *Nature Machine Intelligence*, 3(10), 905–913, 2021.
- [25] B. Yin, F. Corradi, and S. M. Bohtë, *Effective and efficient computation with multiple-timescale spiking recurrent neural networks*, in *International Conference on Neuromorphic Systems 2020*, pp. 1–8, July 2020.
- [26] Y. Xing, G. Di Caterina, and J. Soraghan, *A new spiking convolutional recurrent neural network (SCRNN) with applications to event-based hand gesture recognition*, *Frontiers in Neuroscience*, 14, 590164, 2020.
- [27] Z. Zhou, Y. Zhu, C. He, Y. Wang, S. Yan, Y. Tian, and L. Yuan, *Spik-former: When spiking neural network meets transformer*, *arXiv preprint arXiv:2209.15425*, 2022.
- [28] M. Yao, J. Hu, Z. Zhou, L. Yuan, Y. Tian, B. Xu, and G. Li, *Spike-driven transformer*, *Advances in Neural Information Processing Systems*, 36, 2024.
- [29] M. Yao, J. Hu, T. Hu, Y. Xu, Z. Zhou, Y. Tian, et al., *Spike-driven transformer v2: Meta spiking neural network architecture inspiring the design of next-generation neuromorphic chips*, *arXiv preprint arXiv:2404.03663*, 2024.
- [30] J. Zhang, B. Dong, H. Zhang, J. Ding, F. Heide, B. Yin, and X. Yang, *Spiking transformers for event-based single object tracking*, in *Proceedings of the IEEE/CVF Conference on Computer Vision and Pattern Recognition*, pp. 8801–8810, 2022.
- [31] L. Cordone, B. Miramond, and P. Thierion, *Object detection with spiking neural networks on automotive event data*, in *2022 International Joint Conference on Neural Networks (IJCNN)*, pp. 1–8, IEEE, July 2022.
- [32] M. Yao, H. Gao, G. Zhao, D. Wang, Y. Lin, Z. Yang, and G. Li, *Temporal-wise attention spiking neural networks for event streams classification*, in *Proceedings of the IEEE/CVF International Conference on Computer Vision*, pp. 10221–10230, 2021.
- [33] C. Dhiman, D. K. Vishwakarma, and P. Agarwal, *Part-wise spatio-temporal attention driven CNN-based 3D human action recognition*, *ACM Transactions on Multimedia Computing, Communications, and Applications*, 17(3), 1–24, 2021.
- [34] S. Zhang, Y. Yang, J. Xiao, X. Liu, Y. Yang, D. Xie, and Y. Zhuang, *Fusing geometric features for skeleton-based action recognition using multilayer LSTM networks*, *IEEE Transactions on Multimedia*, 20(9), 2330–2343, 2018.
- [35] J. Liu, A. Shahroudy, D. Xu, A. C. Kot, and G. Wang, *Skeleton-based action recognition using spatio-temporal LSTM network with trust gates*, *IEEE Transactions on Pattern Analysis and Machine Intelligence*, 40(12), 3007–3021, 2017.
- [36] W. Zheng, L. Li, Z. Zhang, Y. Huang, and L. Wang, *Relational network for skeleton-based action recognition*, in *2019 IEEE International Conference on Multimedia and Expo (ICME)*, pp. 826–831, IEEE, July 2019.
- [37] Y. Liu, H. Zhang, Y. Li, K. He, and D. Xu, *Skeleton-based human action recognition via large-kernel attention graph convolutional network*, *IEEE Transactions on Visualization and Computer Graphics*, 29(5), 2575–2585, 2023.
- [38] Z. Wu, P. Sun, X. Chen, K. Tang, T. Xu, L. Zou, et al., *SelfGCN: Graph Convolution Network With Self-Attention for Skeleton-Based Action Recognition*, *IEEE Transactions on Image Processing*, 2024.
- [39] Z. Wu, Y. Ding, L. Wan, T. Li, and F. Nian, *Local and global self-attention enhanced graph convolutional network for skeleton-based action recognition*, *Pattern Recognition*, 111106, 2024.
- [40] H. Tian, Y. Zhang, H. Wu, X. Ma, and Y. Li, *Multi-scale sampling attention graph convolutional networks for skeleton-based action recognition*, *Neurocomputing*, 128086, 2024.
- [41] J. Xie, Q. Miao, R. Liu, W. Xin, L. Tang, S. Zhong, and X. Gao, *Attention adjacency matrix based graph convolutional networks for skeleton-based action recognition*, *Neurocomputing*, 440, 230–239, 2021.
- [42] L. Shi, Y. Zhang, J. Cheng, and H. Lu, *Skeleton-based action recognition with multi-stream adaptive graph convolutional networks*, *IEEE Transactions on Image Processing*, 29, 9532–9545, 2020.
- [43] J. Lee, M. Lee, D. Lee, and S. Lee, *Hierarchically decomposed graph convolutional networks for skeleton-based action recognition*, in *Proceedings of the IEEE/CVF International Conference on Computer Vision*, pp. 10444–10453, 2023.
- [44] R. Hang and M. Li, *Spatial-temporal adaptive graph convolutional network for skeleton-based action recognition*, in *Proceedings of the Asian Conference on Computer Vision*, pp. 1265–1281, 2022.
- [45] D. Tal and E. L. Schwartz, *Computing with the leaky integrate-and-fire neuron: logarithmic computation and multiplication*, *Neural Computation*, 9(2), 305–318, 1997.
- [46] A. L. Hodgkin and A. F. Huxley, *A quantitative description of membrane current and its application to conduction and excitation in nerve*, *The Journal of Physiology*, 117(4), 500, 1952.
- [47] Y. Wu, L. Deng, G. Li, J. Zhu, and L. Shi, *Spatio-temporal backpropagation for training high-performance spiking neural networks*, *Frontiers in Neuroscience*, 12, 331, 2018.

- [48] L. Cordone, B. Miramond, and S. Ferrante, *Learning from event cameras with sparse spiking convolutional neural networks*, in *2021 International Joint Conference on Neural Networks (IJCNN)*, pp. 1–8, IEEE, July 2021.
- [49] A. Zhang, X. Li, Y. Gao, and Y. Niu, *Event-driven intrinsic plasticity for spiking convolutional neural networks*, *IEEE Transactions on Neural Networks and Learning Systems*, 33(5), 1986–1995, 2021.
- [50] A. Vicente-Sola, D. L. Manna, P. Kirkland, G. Di Caterina, and T. J. Bihl, *Spiking Neural Networks for event-based action recognition: A new task to understand their advantage*, *Neurocomputing*, 611, 128657, 2025.
- [51] L. Y. Niu, Y. Wei, W. B. Liu, J. Y. Long, and T. H. Xue, *Research progress of spiking neural network in image classification: a review*, *Applied Intelligence*, 53(16), 19466–19490, 2023.
- [52] A. Shahroudy, J. Liu, T. T. Ng, and G. Wang, *NTU RGB+D: A large scale dataset for 3D human activity analysis*, in *Proceedings of the IEEE Conference on Computer Vision and Pattern Recognition*, pp. 1010–1019, 2016.
- [53] J. Liu, A. Shahroudy, M. Perez, G. Wang, L. Y. Duan, and A. C. Kot, *NTU RGB+D 120: A large-scale benchmark for 3D human activity understanding*, *IEEE Transactions on Pattern Analysis and Machine Intelligence*, 42(10), 2684–2701, 2019.
- [54] J. Wang, X. Nie, Y. Xia, Y. Wu, and S. C. Zhu, *Cross-view action modeling, learning and recognition*, in *Proceedings of the IEEE Conference on Computer Vision and Pattern Recognition*, pp. 2649–2656, 2014.
- [55] Fang, W., Chen, Y., Ding, J., Chen, D., Yu, Z., Zhou, H., Ding, H., & Xie, X., *SpikingJelly: An open-source deep learning framework for spiking neural networks*, Available at: <https://github.com/fangwei123456/SpikingJelly>, 2023.
- [56] Adam Paszke, Sam Gross, Francisco Massa, Adam Lerer, James Bradbury, Gregory Chanan, Trevor Killeen, Zeming Lin, Natalia Gimelshein, Luca Antiga, Alban Desmaison, Andreas Kopf, Edward Yang, Zach DeVito, Martin Raison, Alykhan Tejani, Sasank Chilamkurthy, Benoit Steiner, Lu Fang, Junjie Bai, and Soumith Chintala, *PyTorch: An Imperative Style, High-Performance Deep Learning Library*, *Advances in Neural Information Processing Systems*, 32, 8024–8035, 2019.
- [57] M. Horowitz, *1.1 Computing’s energy problem (and what we can do about it)*, in *2014 IEEE International Solid-State Circuits Conference Digest of Technical Papers (ISSCC)*, pp. 10–14, IEEE, February 2014.
- [58] R. Vemulapalli, F. Arrate, and R. Chellappa, *Human action recognition by representing 3D skeletons as points in a Lie group*, in *Proceedings of the IEEE Conference on Computer Vision and Pattern Recognition*, pp. 588–595, 2014.
- [59] Z. Liu, H. Zhang, Z. Chen, Z. Wang, and W. Ouyang, *Disentangling and unifying graph convolutions for skeleton-based action recognition*, in *Proceedings of the IEEE/CVF Conference on Computer Vision and Pattern Recognition*, pp. 143–152, 2020.
- [60] Y. Fang, Z. Wang, L. Zhang, J. Cao, H. Chen, and R. Xu, *Spiking wavelet transformer*, in *European Conference on Computer Vision*, pp. 19–37, Springer, Cham, 2025.
- [61] J. Wang, Z. Liu, Y. Wu, and J. Yuan, *Learning actionlet ensemble for 3D human action recognition*, *IEEE Transactions on Pattern Analysis and Machine Intelligence*, 36(5), 914–927, 2013.
- [62] S. Song, C. Lan, J. Xing, W. Zeng, and J. Liu, *An end-to-end spatio-temporal attention model for human action recognition from skeleton data*, in *Proceedings of the AAAI Conference on Artificial Intelligence*, Vol. 31, No. 1, February 2017.
- [63] V. Veeriah, N. Zhuang, and G. J. Qi, *Differential recurrent neural networks for action recognition*, in *Proceedings of the IEEE International Conference on Computer Vision*, pp. 4041–4049, 2015.